

# Transcranial Direct Current Stimulation Facilitates Associative Learning and Alters Functional Connectivity in the Primate Brain

Matthew R. Krause,<sup>1</sup> Theodoros P. Zanos,<sup>2</sup> Bennett A. Csorba,<sup>1</sup> Praveen K. Pilly,<sup>3,5,\*</sup> Jaehoon Choe,<sup>3</sup> Matthew E. Phillips,<sup>3</sup> Abhishek Datta,<sup>4</sup> and Christopher C. Pack<sup>1,\*</sup>

<sup>1</sup>Montreal Neurological Institute, McGill University, Montreal, QC H3A 2B4, Canada

<sup>2</sup>Feinstein Institute for Medical Research, Manhasset, NY 11030, USA

<sup>3</sup>Information and Systems Sciences Laboratory, HRL Laboratories, LLC, Malibu, CA 90265, USA

<sup>4</sup>Soterix Medical, Inc., New York, NY 10001, USA

<sup>5</sup>Lead Contact

\*Correspondence: [pkpilly@hrl.com](mailto:pkpilly@hrl.com) (P.K.P.), [christopher.pack@mcgill.ca](mailto:christopher.pack@mcgill.ca) (C.C.P.)

<https://doi.org/10.1016/j.cub.2017.09.020>

## SUMMARY

There has been growing interest in transcranial direct current stimulation (tDCS), a non-invasive technique purported to modulate neural activity via weak, externally applied electric fields. Although some promising preliminary data have been reported for applications ranging from stroke rehabilitation to cognitive enhancement, little is known about how tDCS affects the human brain, and some studies have concluded that it may have no effect at all. Here, we describe a macaque model of tDCS that allows us to simultaneously examine the effects of tDCS on brain activity and behavior. We find that applying tDCS to right prefrontal cortex improves monkeys' performance on an associative learning task. While firing rates do not change within the targeted area, tDCS does induce large low-frequency oscillations in the underlying tissue. These oscillations alter functional connectivity, both locally and between distant brain areas, and these long-range changes correlate with tDCS's effects on behavior. Together, these results are consistent with the idea that tDCS leads to widespread changes in brain activity and suggest that it may be a valuable method for cheaply and non-invasively altering functional connectivity in humans.

## INTRODUCTION

Interest in transcranial direct current stimulation (tDCS) has increased rapidly in recent years, in parallel with growing demand for a low-cost and effective method of modulating brain activity. In a typical tDCS application, electrodes are placed on the scalp, and weak DC current (1–2 mA) is passed through them. This generates an electric field, which is thought to pass through the scalp and skull and to influence the activity of nearby neural tissue. Human behavioral studies report that

tDCS ameliorates several clinical conditions and improves functions ranging from sensation to cognition to emotion [1–4]. These promising findings have led to a large clinical literature on tDCS [1, 5], as well as over 530 clinical trials (according to <https://clinicaltrials.gov/>). However, many behavioral studies have been questioned on statistical and methodological grounds [3, 6–8], though these analyses have themselves been criticized [9, 10].

Furthermore, little is known about the neuronal effects of tDCS. Both *in vivo* and *in vitro* studies have shown that the static electric fields produced by direct current modulate neuronal membrane potentials [11]. However, absent other sources of excitation, the fields produced by tDCS are typically too weak to directly generate action potentials [11], especially after being attenuated by skull tissue and distorted by brain convolutions. Instead, some studies have suggested that tDCS might alter neural excitability [12, 13], brain oscillations [14, 15], or functional connectivity [2, 16]. The few studies that have recorded neuronal data along with tDCS used small animals and invasive stimulation paradigms that cannot be applied to humans (e.g., stimulating through screws driven deep into the skull) [17–20]. Thus, fundamental questions about the nature and efficacy of tDCS remain.

To investigate these issues, we applied stimulation techniques and equipment intended for human use, combined with large-scale neurophysiological recordings from awake, behaving macaque monkeys. Macaques are an ideal model system for this because, like humans—and unlike other animal models—they have a thick, dense skull and gyrencephalic cortex, which may affect the strength and flow of current into the brain [11, 21]. Macaques also learn complex behaviors, permitting a direct comparison with human experiments and real-world conditions. At the same time, using an animal model permits a more detailed examination of neural activity than is possible in healthy human subjects.

Our experiments sought to answer two questions: first, what effects (if any) does tDCS have on activity in the primate brain? To answer this question, we recorded local field potential (LFP), multi-unit activity (MUA), and single-neuron activity at multiple sites within the neocortex of two monkeys. Second, do the observed neural effects influence behavior? To answer this

question, we trained the monkeys to perform a task that required them to learn new associations between stimuli and behavioral responses. We then asked whether aspects of neural activity correlated with performance on this task, and whether tDCS modulated these aspects.

We find that tDCS has both local and widespread effects on brain activity. The local effects consist primarily of an increase in LFP power near the site of anodal stimulation. The more widespread effects are manifested as a decrease in low-frequency LFP coherence between distant cortical sites, along with an increase in high-frequency (gamma-band) coherence between the same sites. Of these effects, the last was most strongly correlated with the animals' behavioral performance, suggesting that, for certain tasks, the beneficial effects of tDCS arise from increased communication and altered functional connectivity between distant brain regions [22].

## RESULTS

### Effects of tDCS on Neural Activity in the Non-human Primate Brain

The metallic implants and skull defects required for neurophysiological recording may distort the electric field generated by tDCS [23], and individual differences in neuroanatomy may also cause electrodes placed on similar scalp locations to generate different electric fields within the brain [24]. To minimize these potential confounds, we first created a detailed finite element model of each monkey's head. The model was then solved to find scalp locations that maximized the electric fields within a targeted brain location [23]. We considered both traditional bipolar electrode montages and montages containing up to 8 stimulating electrodes. Since the vast majority of human experiments use no more than 2 mA of stimulating current, we also limited our montages to 2 mA total current. We generated electrode montages that maximized field strength in right lateral prefrontal cortex (PFC), an area with extensive neuroanatomical connections [25], associated with memory formation and recall [26], and the focus of many human tDCS studies. The finite-element models indicate that these montages generated fields of 0.68 V/m in PFC of one monkey and 0.42 V/m in the other. These values are comparable to those estimated for healthy human subjects (0.4–1.0 V/m from [11, 27]) and measured in human epilepsy patients (0.4 V/m from [28]). Further details of the modeling procedure, including the models generated for the animals used in this study, have already been published [23]; Figure S1 shows the field strength for one animal.

Since virtually nothing is known about the effects of tDCS on the primate brain, we first sought to determine whether it affects neural activity. Two non-human primates were each implanted with a pair of 96-channel "Utah" arrays: one in the right PFC and the other in the left inferotemporal cortex (ITC). Animals were trained to sit calmly in a darkened testing chamber while fixating a small target displayed against a gray background; liquid rewards were dispensed every 1–3 s while the animal maintained fixation. This task allowed us to control the animals' behavioral and oculomotor state across stimulation conditions.

The design of this experiment is shown in Figures 1A and 1B. Animals continuously performed the fixation task while two types of electrical stimulation were applied in 5-min blocks. These

blocks were randomly ordered and separated by 5- to 10-min interstimulus intervals. In a tDCS block, the current was gradually ramped up from 0 to 2 mA over 3 s, maintained at 2 mA for 5 min, and then ramped down from 2 to 0 mA over 3 s. Less than 1% of human subjects can detect the presence or absence of a 2-mA DC current on the scalp at steady state, but its onset and offset generate noticeable somatosensory percepts [30, 31]. We therefore compared our tDCS data against the "sham" stimulation protocol in Figure 1A. As in the active protocol, stimulation was initially ramped up from 0–2 mA over 3 s. However, in sham blocks, the full 2-mA current was only applied for 10 s and then ramped back down to zero over 3 s. At the end of a sham block, the 2-mA current was again applied and ramped back down to 0 mA. This protocol generates the same somatosensory percepts as the active condition but passes far less charge into the brain. Since blinded human subjects are typically unable to report whether they received active or sham stimulation [18, 32], this tDCS versus sham comparison is currently the gold standard for human neurostimulation research [33].

Figure 1A shows representative signals from electrodes in PFC (left) and ITC (right). When tDCS is applied to PFC (yellow), large, low-frequency oscillations appear in the underlying LFPs. LFPs provide a sensitive measure of neural excitability by tracking membrane potential fluctuations within a few hundred micrometers of the electrode tip [34]. These larger oscillations do not appear during sham stimulation (blue) in PFC, nor do they appear in ITC in any condition when PFC is targeted.

To test for these effects' specificity, we also generated a second montage, which targeted left ITC. When tDCS was applied according to this montage (Figure 2B, yellow), it induced low-frequency oscillations within ITC, but not PFC. Again, these results were markedly different from what was seen during sham stimulation (blue) with the same montage and were not seen in the non-targeted region (PFC). As the field map in Figure S1 shows, regions around the target, particularly those between the anodal and cathodal electrodes, also receive some stimulation. However, this spatial specificity is incompatible with global arousal changes related to the somatosensory sensations evoked by tDCS's onset.

These results provide a proof of principle that tDCS, delivered through the scalp, can influence neural activity in the primate brain. However, because the effects of tDCS may vary with behavioral state [35], we next analyzed data collected from PFC and ITC while the monkeys performed a challenging behavioral task. We first consider the effects of tDCS on behavior, and then we ask whether these behavioral effects could be mediated by tDCS-induced changes in local or widespread neural activity.

### Effects of tDCS on Performance in an Associative Learning Task

Two non-human primates were trained to perform an oculomotor foraging task [29] depicted in Figure 1C. This task requires learning arbitrary associations between natural images and response zones (RZs), small ( $2^\circ$  radius) regions within each image. On each trial, animals were shown a single image and allowed to freely view it. When they fixated within the RZ for 100 ms, they received a juice reward, and the trial ended. Presentations of 2–3 images, each with its own RZ, were randomly interleaved. Each image's RZ was randomly chosen at the start

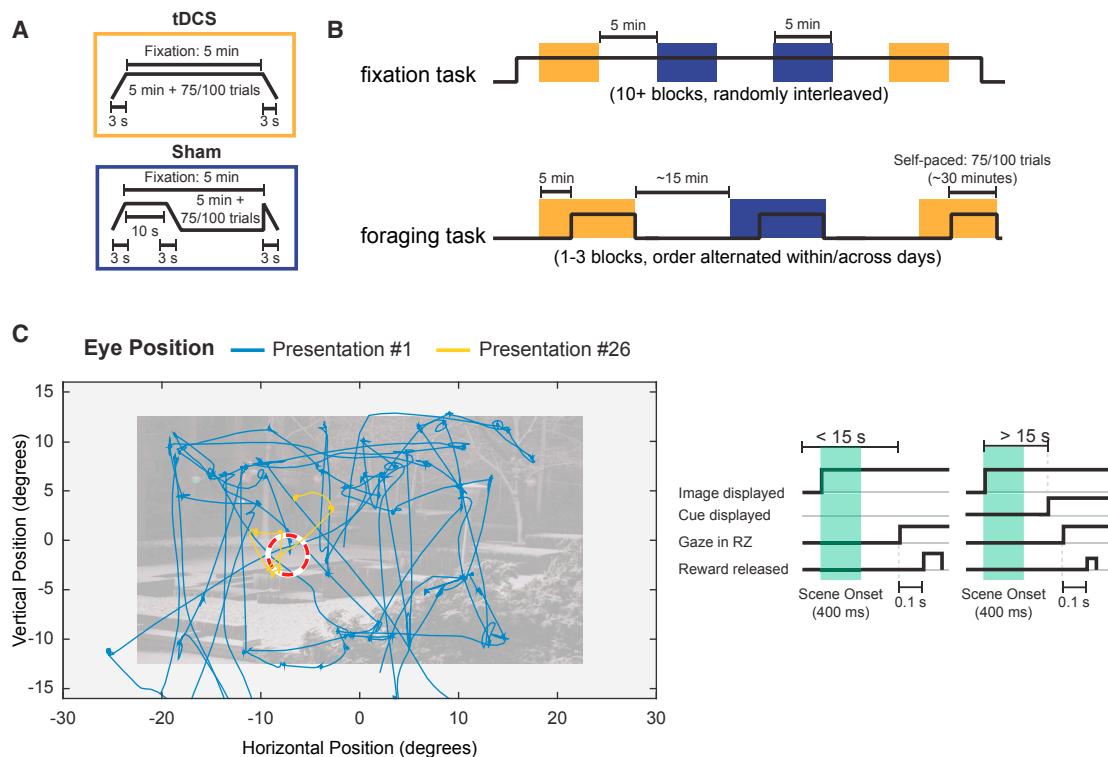


**Figure 1. Experimental Design**

(A) Data from two stimulation conditions, active tDCS and sham stimulation, are compared in the following experiments. (A) Waveforms for tDCS (yellow box) and sham stimulation (blue) are shown. The peak current in both conditions was 2 mA. Please see Figure S1 for a depiction of the induced electrical field.

(B) (top) In the passive fixation experiment (see text and Figure 2), tDCS (yellow) and sham (blue) stimulation were applied in 5-min blocks, separated by a 5-min interstimulus interval. Blocks were randomly ordered and at least 10 blocks were collected each day. (bottom) During the foraging paradigm (see text and C), tDCS and sham stimulation were applied for 5 min before the task began and then continued until the monkey performed 75 (monkey F) or 100 (monkey M) trials of each image. Trials were separated by 500–1,000 ms, while tDCS and sham blocks were separated by 15-min intervals. One to three blocks were performed each day, and the tDCS/sham order was alternated within sessions and across days (e.g., since the session shown here began with a tDCS block, the next session would start with a sham block, followed by a tDCS one).

(C) A naturalistic foraging task [29] was used to study the effects of tDCS on associative learning. (left) Animals learned to associate an image (contrast reduced for illustration) with a reward zone, which is shown here by a red and white ring, although the ring was not displayed during the experiments. Animals initially explored the entire image but after repeated experience learned to saccade directly to the reward zone. The overlaid traces are one animal's eye movements during his initial exposure to this image/location pair (blue) and 25 trials later (yellow). (right) On each trial, we evaluated neural data from the 400 ms following scene onset (scene onset epoch). Animals learned two or three image pairs per session. During each session, tDCS or sham stimulation was applied to PFC, as described in (A) and (B).

of the block, and, except for a small jitter ( $0\text{--}4^\circ$ ), its location was fixed across presentations of the same image.

Along with the foraging task, animals also performed a simple visually guided saccade-to-target task. On these trials, animals were shown a gray screen containing only a small, high-contrast saccade target. They received a small liquid reward for saccading to the target and maintaining their gaze on it for 750–1,250 ms. This is essentially the same paradigm used in the passive fixation experiment (above), except that the target location was randomly chosen from one of 9 (or 25) locations on a  $3 \times 3$  (or  $5 \times 5$ ) grid spanning the monitor. Since these trials were intended to monitor the animals' motivation and ensure that the eye tracker remained calibrated, they were interleaved so at least one saccade-to-target trial followed every foraging trial.

To study the effects of tDCS, each block was paired with either active tDCS or sham stimulation; conditions were counterbal-

anced within and across days to avoid order effects (Figure 1B). At the beginning of each block, the stimulation was applied for 5 min while the animals sat quietly. We then began the behavioral paradigm depicted in Figure 1C. Both the behavioral paradigm and stimulation ended after every image was shown 75 (monkey F) or 100 (monkey M) times. Since the trials were self-paced, blocks varied in length. The median stimulation length was 35 min and never exceeded 1 hr.

We used the response time (RT), defined as the time elapsed between the scene onset and the successful localization of the RZ, to measure performance. Early in a block, animals explored the entire image before finding the RZ (Figure 1C, blue). However, after repeated presentations, they learned to saccade directly into the RZ (Figure 1C, yellow), indicating that they learnt to associate images with their corresponding RZs. Plotting the RT versus presentation number revealed that this change in RT approximated a sigmoidal trajectory (Figure 3A). Accordingly,

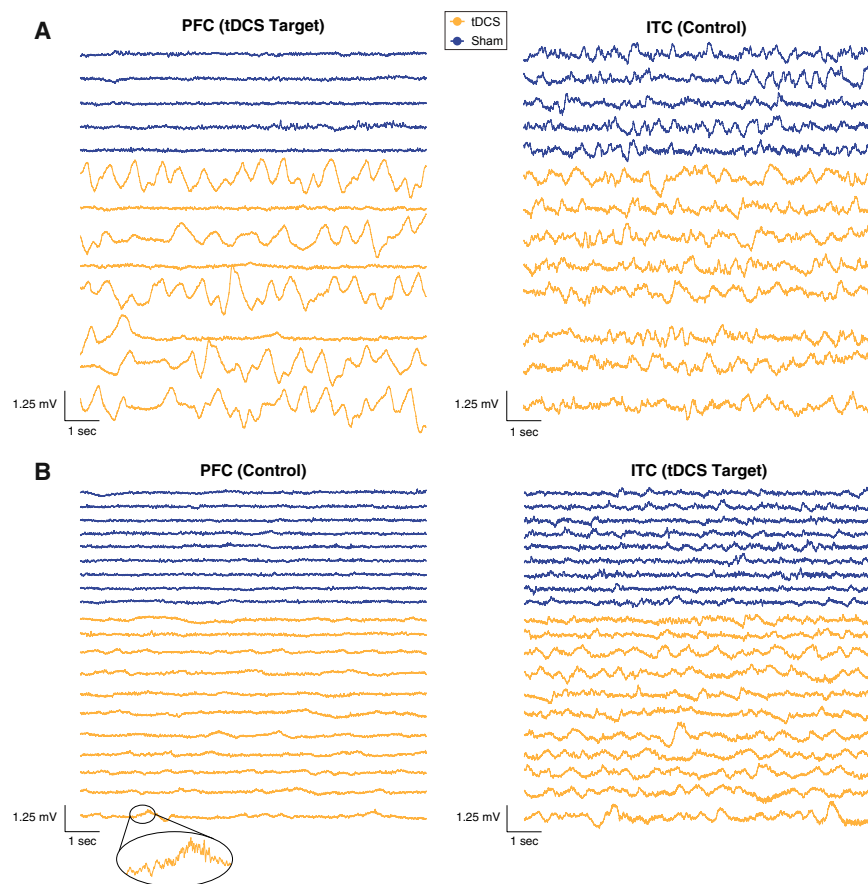


**Figure 2. Influence of tDCS on Raw LFP Signals**

Applying tDCS produces large low-frequency oscillations in the targeted brain area. Traces show unprocessed, wideband signals simultaneously recorded from electrodes in PFC (left) and ITC (right) during tDCS (yellow) and sham stimulation (blue). Stimuli were applied for 5 min; the last 10 s of each block (before ramp-down) is shown here. Blocks were randomly ordered during the experiment, but traces have been grouped by condition here for display.

(A) In blocks where tDCS is applied to PFC (yellow traces, left side), large low-frequency oscillations are present in the LFP recorded from PFC. These are not present in PFC during sham stimulation (blue traces, left side), nor are they present in ITC during either condition (yellow and blue traces, right side).

(B) When tDCS is instead applied to ITC, oscillations become visible in ITC (right), but not PFC (left), instead. As in (A), this is restricted only to active tDCS (yellow), not sham (blue), and only within the targeted brain area (right).

One prosaic explanation for these effects is that tDCS may cause non-specific changes in arousal, causing the monkeys to physically perform the task more rapidly. Although this seems unlikely based on the human data mentioned above [18, 32], we performed several additional control analyses. First, we

we fit the RT versus presentation number data for each image/RZ pair to a logistic function (see STAR Methods). This parameterization separates potential effects of tDCS on associative learning from sensory [20] or motor [36] effects. Sensorimotor effects (e.g., faster scene recognition) would affect performance before and after learning equally, leading to vertical shifts of the RT curve, while changes in learning efficiency would be reflected in horizontal shifts of the curve.

These possibilities were examined by fitting data from 75 experimental sessions (38 tDCS, 37 sham) to logistic functions and analyzing the corresponding parameters (see STAR Methods). The logistic functions generally fit the data very well ( $r^2 = 0.83$ ), with no significant difference in fit quality across stimulation conditions (tDCS: 0.82; sham: 0.85;  $p = 0.625$  via Fisher-Pittman test). First, we examined the  $N_{50}$  parameter, which shifts the logistic RT curve horizontally. Smaller values of  $N_{50}$  indicate that the animals learned more efficiently, or equivalently, fewer trials were required for animals to reach their asymptotic performance. Applying tDCS significantly reduced  $N_{50}$ , from  $20.9 \pm 3.6$  trials during sham stimulation to  $12.0 \pm 1.4$  trials ( $M \pm SE$ ) during tDCS ( $p = 0.019$ ; Fisher-Pittman test), as shown in Figure 3B (left). Randomized F-test indicated that there was no main effect ( $p = 0.18$ ) or interaction ( $p = 0.42$ ) with monkey identity. These data suggest that tDCS accelerated the monkeys' ability to learn new associations. This effect could have been underestimated, as prolonged exposure to neurostimulation, even within the same experiment [37], can reduce its efficacy.

examined the *MinRT* parameter, which controls the vertical position of the RT curve, and represents the time needed to execute a response after learning (time required for recognizing the image, planning and executing saccades, etc.). Figure 3B (right) shows that the *MinRT* values were similar for the tDCS and sham conditions (tDCS:  $M \pm SE = 1.43 \pm 0.1$  s; sham:  $1.38 \pm 0.1$ ). Neither a Fisher-Pittman randomization test ( $p = 0.69$ ) nor a randomized F-test with a per-monkey factor (main effect of stimulation  $p = 0.39$ ; main effect of monkey:  $p = 0.54$ ; interaction:  $p = 0.43$ ) revealed any difference in *MinRT* values between stimulation conditions. Monkeys can execute visually guided saccades in approximately 200 ms [38], so it is unlikely that a floor effect masked possible effects of tDCS on arousal, sensory processing, or similar factors related to task execution.

Second, we examined RT data from the saccade-to-target trials, which have no learning or memory components. Instead, the RTs are determined by the speed with which the monkey detects the target's onset and plans/executes saccades toward it. We defined the RT for this task as the time elapsed between saccade target onset and the monkeys' gaze landing within  $2^\circ$  of the target. These RTs did not significantly differ between tDCS blocks ( $M \pm SE: 546 \pm 13$  ms) and sham blocks ( $M \pm SE: 539 \pm 20$  ms), according to a Fisher-Pittman test ( $p = 0.99$ ) and a two-way randomized F-test with a per-monkey covariate (main effect of stimulation  $p = 0.83$ ; main effect of monkey:  $p = 0.24$ ; interaction  $p = 0.43$ ). Monkeys were not trained or incentivized to respond rapidly in this part of the task. Reaction

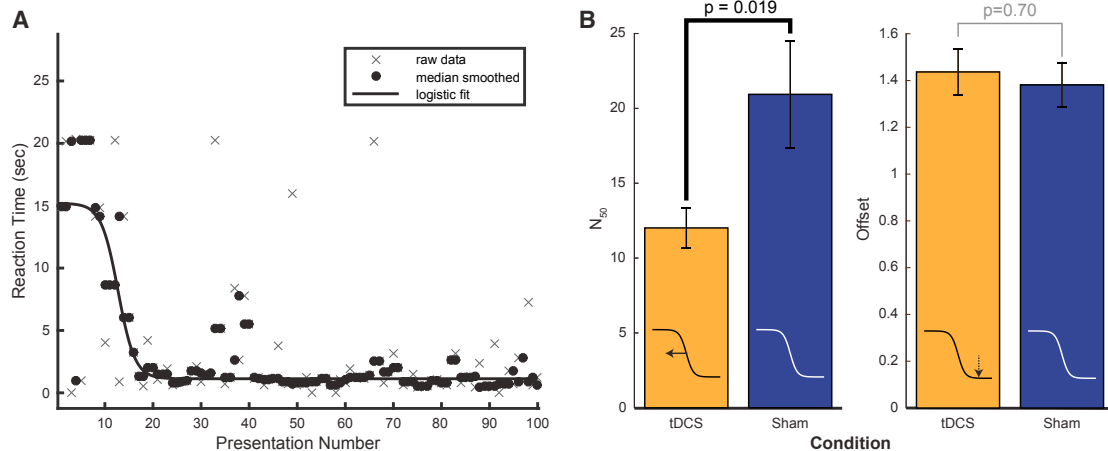


### Figure 3. Behavioral Results

(A) As the example in Figure 1A suggests, animals' RTs decreased over the course of the session. Since this decrease appeared to be sigmoidal, we fit logistic functions to each sessions' data. They generally fit the data well ( $r^2 = 0.83$ ), and this did not significantly differ by condition (tDCS: 0.82; sham: 0.85;  $p = 0.625$  via F-P randomization test). Two parameters corresponding to aspects of task performance were extracted. Downward shifts of the curve, governed by the *MinRT* parameter, suggest that animals perform the task faster once learning is complete, while leftward shifts, indicated by changes to the  $N_{50}$  parameter, suggest that animals learn more efficiently.

(B) (left) The  $N_{50}$  parameter was significantly smaller in sessions in which tDCS was applied, suggesting that tDCS improves associative learning efficiency. However, we found no difference in the *MinRT* parameter, indicating that tDCS does not alter the speed with which the monkeys respond after learning. This suggests that tDCS does not increase animals' arousal levels (see main text and Figure S2). Error bars represent SEM.

times were therefore relatively slow so, as described above, it is unlikely that a tDCS-mediated effect is masked by floor effects here either. This result is in contrast to previous work showing a relationship between arousal [39] or attention [38, 40, 41] and saccade initiation.

Finally, we looked for tDCS-mediated changes in pupil size, a well-known biomarker for arousal and attentional state [42, 43]. For this analysis, we returned to the passive fixation paradigm described above because the visual stimulus and eye positions remained constant throughout the entire experiment. Changes in pupil area are therefore likely to reflect only changes in arousal or attention. Pupil area was recorded throughout the experiment and divided into three epochs: a baseline period containing the 2 min before each tDCS/sham application, a "ramp" period containing the 6 s surrounding stimulation onset, and a "steady-state" period containing the second half of the stimulation block. Data from each epoch were summarized using the median because it is robust against blinks and other outliers.

Pupil area trajectories are shown in Figure S2. Compared with the baseline period, pupil area was significantly increased during the subsequent ramp periods ( $\Delta M \pm SE$ :  $74 \pm 19$  arbitrary units,  $p < 0.0001$ , matched-sample Fisher-Pittman test;  $n = 27$ ). However, this increase was short lived: pupil size significantly decreased from the ramp to subsequent steady-state periods ( $\Delta M \pm SE$ :  $-60 \pm 20$  a.u.,  $p < 0.0001$ , matched-sample Fisher-Pittman test). This represents a return to baseline, because pupil size was *not* significantly different from baseline during the steady-state period ( $\Delta M \pm SE$ :  $-14 \pm 12$  a.u.,  $p = 0.42$ , matched-sample Fisher-Pittman test;  $n = 27$ ). Critically, the baseline to steady-state difference was also not influenced by the choice of tDCS or sham stimulation ( $\Delta M \pm SE$ :  $-12 \pm 14$

a.u. for tDCS,  $-17 \pm 23$  for sham,  $p = 0.22$ , Fisher-Pittman test,  $n = 11$  and 16). These data parallel subjective reports from human subjects, where only the onset of current flow is perceptible, and further support the idea that tDCS does not lead to non-specific changes in attention or arousal.

### Local Effects of tDCS on Neural Activity during Task Performance

We examined neural activity during the 400 ms following the onset of the image within each trial (Figure 1C). This epoch was chosen to avoid potential artifacts from saccade-related modulation of the LFP signals [44]; results (data not shown) were similar during other trial epochs.

To simplify the analysis, we divided the LFP signals into six standard frequency bands (delta: 2–4 Hz; theta: 4–8 Hz; alpha: 8–12 Hz; beta: 16–24 Hz; low gamma: 24–40 Hz; high gamma: 40–100 Hz). As during passive fixation (Figure 2), in PFC, tDCS led to large increases in LFP power during performance of the behavioral task (Figure 4A). We observed significant changes in LFP power across all frequency bands ( $p < 0.05$ , individual Fisher-Pittman and randomized F tests, corrected). These effects were not evident in any frequency band in ITC (Figure 4B;  $p > 0.05$ , individual Fisher-Pittman and F tests, corrected), suggesting that the application of tDCS produced a non-specific amplification of neural oscillations only within the targeted brain area. Since electrodes had somewhat different impedances, these results were confirmed with a randomized *F*-test incorporating an array-specific factor.

Applying tDCS had similar effects on intra-areal coherence: we observed a significant increase in local coherence within PFC in all frequency bands (Figure S4A,  $p < 0.05$ ; corrected, individual Fisher-Pittman tests), but stimulation produced no

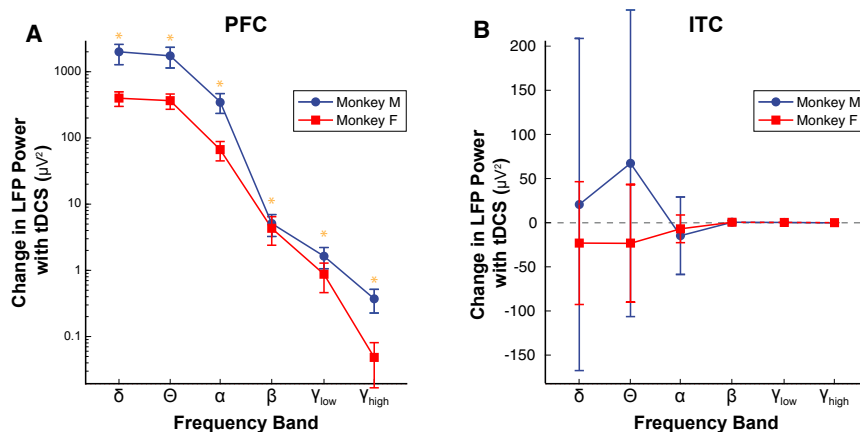


**Figure 4. tDCS of PFC Affects LFP Spectral Power**

(A) In PFC, tDCS led to a broadband increase in spectral power (all bands:  $p < 0.05$ ), compared to sham stimulation. Due to the range of the data, this panel is plotted on a log scale for the y axis. (B) No stimulation-evoked changes were observed in ITC (data shown here on a linear scale). Statistical tests reported in the text were performed on all data by including a covariate for arrays. \*Pairwise differences that are significant at a corrected 0.05 level. Average spectral power values for one monkey are shown in Figure S3. Error bars represent SEM.

significant changes in the average coherence between pairs of ITC electrodes (Figure S4B;  $p > 0.05$ , corrected). These data suggest that tDCS provides a strong common input to the stimulated area.

We also looked for effects of tDCS on single-unit firing rates (Figure 5A). Overall there was no consistent effect on firing rates in PFC ( $p = 0.07$ ) or ITC ( $p = 0.3$ ; randomized F-tests). There was also no effect of tDCS on selectivity for the visual scenes in the foraging task (Figure 5B;  $p = 0.49$  in PFC,  $p = 0.30$  in ITC). Similarly, MUA was not modulated in either area by tDCS (Figure 5A; PFC:  $p = 0.43$ ; ITC  $p = 0.29$ ). There was a tendency for tDCS to decrease MUA selectivity for visual images in both areas, but it did not reach statistical significance (PFC:  $p = 0.55$ ; ITC;  $p = 0.33$ ), as shown in Figure 5B.

In summary, the local effects of tDCS consisted of a broadband increase in LFP power and coherence in the targeted region (PFC), with no effect on single-unit or MUA firing rate or selectivity.

### Widespread Effects of tDCS on Neural Activity

Next, we sought to characterize the effects of tDCS on functional connectivity between brain regions [16]. We computed LFP-LFP coherence, a standard measure of functional connectivity [45, 46], between all pairs of electrodes in PFC and ITC. Figure 6 summarizes the difference between inter-areal coherence for the tDCS and sham conditions: positive values indicate increased coherence during tDCS. The results show that tDCS sharply decreased coherence at lower frequencies, with significant decreases being observed in alpha and theta bands (individual Fisher-Pitman tests;  $p < 0.05$  corrected). At the same time, coherence increased at higher frequencies: significant effects were observed in low- and high-gamma bands ( $p < 0.05$ ; corrected). Thus, tDCS directed to PFC altered functional connectivity between PFC and ITC.

Since single-unit firing rates were generally too low (<1–2 spikes per epoch, as shown in Figure 5) for reliable estimation of spike-field coherence (SFC), we used the multiunit activity, which has been shown to reliably estimate single-neuron interactions [47]. The results (Figure 7) show a sharp decrease in SFC between MUA in each area and the LFP in the other area. Specifically, SFC decreased significantly in the delta and theta bands (Fisher-Pitman tests;  $p < 0.05$ ,

corrected). Changes in beta and high gamma were individually significant but did not survive multiple comparisons correction. Together, these results suggest that tDCS significantly altered inter-areal coherence in various frequency bands.

### Behavioral Correlates of tDCS-Induced Changes in Neural Activity

The previous sections demonstrated that tDCS improves behavioral performance (Figure 3) and alters both local and long-range neural activity. To connect these two effects, we examined session-to-session fluctuations in the animals' behavioral and neural activity. Specifically, we asked whether generalized linear models (GLMs) using LFP power (Figure 4) and coherence (Figures 6 and S4) could explain changes in learning speed, as measured by the  $N_{50}$  behavioral parameter. Bayesian Information Criterion (BIC) values were calculated for each model. Since lower BIC values correspond to better model parsimony (i.e., goodness of fit, corrected for model complexity), when BIC increases after a predictor is removed it suggests that that predictor carries information about the response variable. BIC changes of  $\sim 10$  units are typically thought to provide strong evidence for the superiority of a model and/or the importance of a predictor.

A model using inter-areal coherence was able to predict performance on the learning task ( $p < 0.01$ ;  $\Delta DF = 10$ ). We found significant main effects of alpha ( $p = 0.003$ ) low-gamma ( $p \leq 0.01$ ), and high-gamma-band inter-areal coherence ( $p < 0.0001$ ). To determine which contributions were most important, we refit GLMs, dropping individual frequency bands. The results showed that removing high-gamma had the largest impact on the model's quality ( $\Delta BIC = 29$ ), followed by low-gamma ( $\Delta BIC = 26$ ). Other frequency bands were less important (all  $\Delta BIC < 22$ ). The relationship between alpha and  $N_{50}$  was positive, suggesting that increases in alpha coherence slow learning. However, the relationship between high-gamma coherence and  $N_{50}$  was negative, indicating that larger high-frequency coherence was associated with faster learning. The remaining models, using spectral power from PFC and ITC, as well as the average coherence within each area, all failed to predict behavioral performance better than the null model ( $p > 0.1$ ,  $\Delta DF = 10$ ).

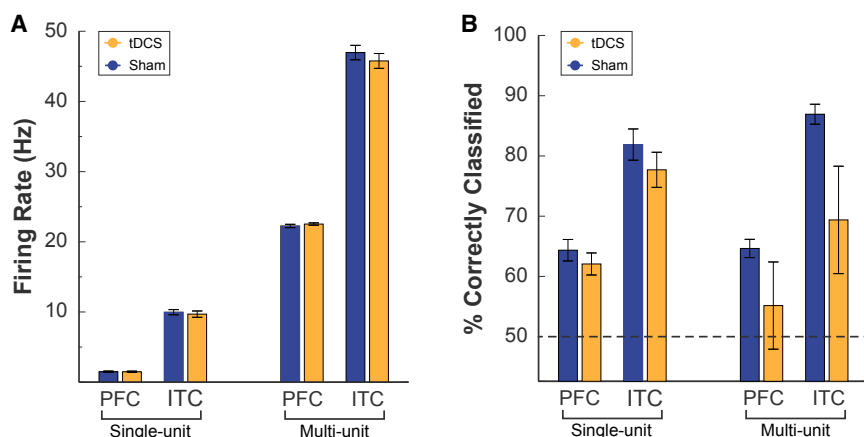


**Figure 5. tDCS Does Not Affect Single-Unit or MUA or Selectivity**

(A) Single-unit and multi-unit firing rates were not significantly different following tDCS (yellow) or sham (blue) stimulation in either area.

(B) The selectivity of single units, as assessed with a linear discriminant analysis, was also not significantly altered by tDCS in either area.

Error bars represent SEM.

To avoid potential spurious correlations during tDCS stimulation, we also limited the model inputs to data collected during sham blocks. Again, a model using inter-areal coherence was able to predict behavioral performance on the learning task better than a model containing only a constant (F versus constant: 5.19;  $p = 0.00126$ ,  $R^2 = 0.54$ ). Examination of the individual predictors confirmed the effect of high gamma ( $p = 0.0003$ ). As before, its coefficient was negative, indicating that increasing high gamma coherence speeds learning.

This role for inter-areal high gamma coherence was again confirmed using a model comparison approach in which we compared the full model, containing all frequency bands, with a series of reduced models in which each predictor was removed in turn. We found that removing high gamma coherence had the largest impact on BIC ( $\Delta\text{BIC} = +16.33$ ), suggesting that this frequency band carries information about  $N_{50}$ . BIC values after dropping the other predictors were essentially unchanged ( $\Delta\text{BIC} = -2.71$  to  $+0.59$ ), and significance tests indicated that the corresponding coefficients were not significantly different from zero ( $p > 0.05$ ). These results suggest that, in the absence of tDCS, endogenous high gamma coherence is associated with improved behavioral performance.

Models using intra-areal coherence within PFC and ITC were not significantly better than a constant model (PFC  $p = 0.741$ , ITC  $p = 0.88$ ). A model using ITC spectral power also failed to predict behavioral performance ( $p = 0.88$ ). However, LFP power in PFC was associated with faster learning (F versus constant: 5.72,  $p = 0.0007$ ). Faster learning was associated with decreased low gamma power ( $p = 0.004$ ) and increased beta ( $p = 0.02$ ) power. However, dropping these predictors had little impact on model quality ( $\Delta\text{BIC} = -2.17$  and  $+3.0$ , respectively). Together these results show that high-gamma inter-areal coherence was the best predictor of learning efficiency. As this measure was also significantly modulated by tDCS (Figure 6), it emerges as the most likely candidate for a mechanistic explanation of the influence of tDCS of associative learning in our task.

## DISCUSSION

One of the most mysterious aspects of tDCS is that a weak electric field, further attenuated by the skull and scalp, still affects

neural activity. The literature contains many hypotheses about the underlying mechanism, but our results are most consistent with the idea that tDCS acts by modulating functional connectivity [2, 16]. Specifically, we find that applying tDCS weakens low-frequency coupling between PFC and ITC, while simultaneously strengthening functional connectivity at higher frequencies. Thus, for learning and memory tasks in particular, prefrontal tDCS might improve performance by improving communication between PFC and other areas [48].

## Neural Correlates of tDCS

Intracellular recordings from slice and small animal preparations indicate that exposure to an external DC electric field depolarizes neurons. This effect may manifest itself in two ways in the brain of an awake, behaving animal (or human). First, it may directly evoke neural firing. Early studies of tDCS reported changes in the firing rate of individual neurons [17, 49]. However, those studies used more current and invasive stimulation approaches. More recent studies, using tDCS comparable to that used here, have shown that the electric field reaching the brain is quite weak, and the resulting depolarization is roughly two orders of magnitude too small to bring neurons from resting to action potential threshold [11]. Our results largely confirm this: the average firing rate of individual neurons is essentially unchanged by tDCS (Figure 5), suggesting that tDCS does not directly elicit action potentials.

Alternatively, the common input generated by tDCS may synchronize membrane potentials in the targeted area [11]. While this could amplify responses to weak inputs, it may also lead to alterations in spike timing [12] without necessarily affecting spike rates. When a neuron is already bombarded with synaptic input, the mild depolarization attributable to tDCS may cause it to fire sooner than it otherwise might, even if the stimulation does not provide enough excitation to evoke additional action potentials. In this case, tDCS would influence oscillatory activity at frequencies determined by the dynamics of the cortical network [50]. Gamma oscillations are common in cortical networks and can entrain oscillations at distant sites [22]. Thus, the previous observations of gamma modulation by tDCS [16, 51] might be an indirect consequence of large-scale polarizations of membrane potential, coupled with gamma-specific dynamics within neural circuits.

Our data show that tDCS causes strong, consistent changes in the LFP, a reliable proxy for nearby cells' membrane potentials [34]. Locally, the strongest effect of tDCS was an increase in low-frequency oscillations (Figures 2 and 4). However, these

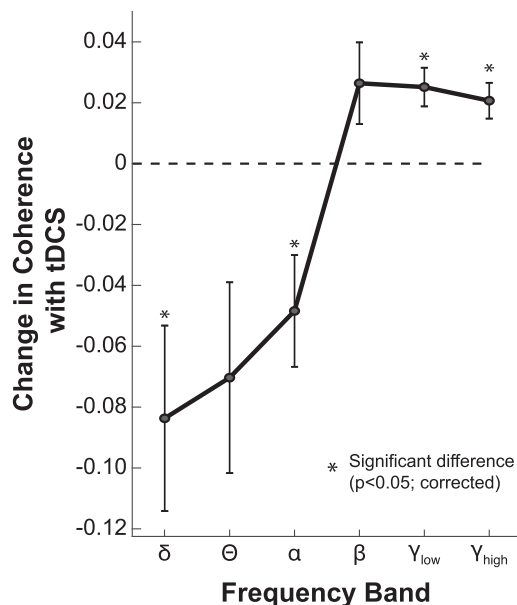


**Figure 6. tDCS Alters Functional Connectivity between Brain Areas**

The difference between LFP-LFP coherence for tDCS and sham conditions. Positive values indicate greater coherence during tDCS, while negative values indicate higher values during sham stimulation. Low-frequency (delta, theta, alpha) coherence decreased during stimulation sessions, while high-frequency coherence increased with stimulation. \*Pairwise differences that are significant at a corrected 0.05 level. Changes in the theta and beta bands trended toward significance ( $p < 0.1$ ) but did not survive multiple comparison corrections. For raw coherence values for each area, please see Figure S5. For coherence within PFC and ITC, please see Figure S4. Error bars represent SEM.

effects cannot be directly linked to improved behavioral performance. Our results (Figures 6 and 7) show that tDCS actually decreases inter-areal coherence at low frequencies, while increasing it at high-frequency bands that are associated with improved task performance. This may be a consequence of the fact (Figures 2 and 4) that low-frequency oscillations are strongly enhanced by tDCS. Since these stimulation-driven effects are relatively local to the targeted area and are uncorrelated with the amplitude and timing of endogenous oscillations, they may effectively decouple the targeted brain area from oscillations at similar frequencies in distant brain regions.

One appealing hypothesis is that tDCS generates low-frequency oscillations within the targeted brain area. These stimulation-evoked oscillations may decouple the targeted area from more widespread oscillations at the same frequency, allowing local computations or more targeted communication (carried in high-frequency bands) to proceed unhindered. Consistent with this idea, inter-areal high gamma coherence and PFC delta power were more correlated during tDCS than sham sessions (Spearman's  $r_{sham} = 0.20$ ,  $r_{stim} = 0.62$ ,  $p = 0.02$ ; r-to-z test).

At the same time, our analysis of LFP-MUA coherence between areas (Figure 7) shows that tDCS primarily has the effect of disrupting the precision of spike timing relative to low-frequency LFP oscillations, with little effect on locking to high-frequency oscillations. Since these low-frequency oscillations tend to be widespread and suppressive, this may render cells

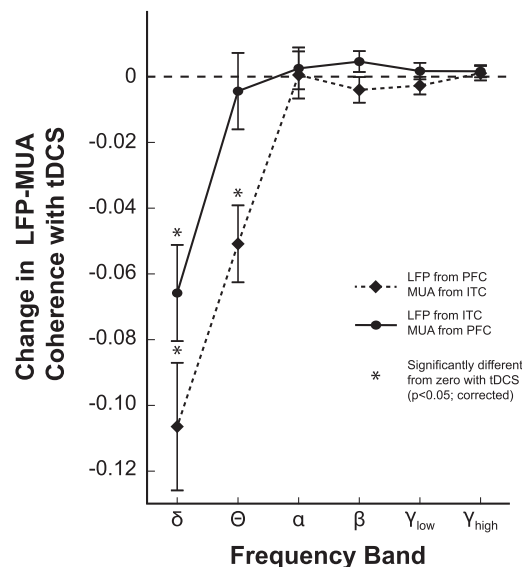


**Figure 7. tDCS Reduces the Locking of Spikes to Low-Frequency Oscillations**

Plot indicates the difference between MUA-LFP coherence for tDCS and sham stimulation for signals between the two brain areas. Positive values indicate greater coherence during tDCS, while negative values indicate higher values during sham stimulation. The results show a significant decrease in coherence between the low-frequency LFPs in each area and the MUAs in the other area. \*Differences that are significantly different from zero at the 0.05 (corrected) level. Error bars represent SEM.

more sensitive local circuit activity, which typically involves higher-frequency oscillations [22]. This conclusion is, however, limited by the fact that we did not have any way of identifying specific sites with direct anatomical connectivity between PFC and ITC, so effects of timing, particularly at higher frequencies, may have been obscured by averaging across sites.

Finally, astrocytes are also thought to play a role in regulating neuronal synchrony [52]. Since astrocytes are particularly susceptible to electrical fields and synchronously release calcium in response to tDCS [53], they may provide another indirect pathway through which tDCS coordinates widespread neural activity.

### Behavioral Consequences of Altered Coherence

Given the hypothesized mechanisms of tDCS, one would not expect its influence to be specific to particular functions. Moreover, since PFC sends anatomical projections to a variety of different brain regions [25], tDCS targeted at this area would likely influence performance on many different tasks. Thus, we do not expect that our observations on inter-areal coherence are specific to PFC and ITC, except insofar as this behavioral task requires processing a complex visual stimulus.

In the associative learning task used here, tDCS appears to accelerate the rate at which animals learn to associate each stimulus with a particular behavior (Figure 3B). Previous work has shown that gamma coherence between PFC and visual cortex is modulated by attention [45], so our experiments may reflect heightened attention to the visual stimulus. However, as mentioned above, heightened attention would influence performance on a simple reaction time task, which is inconsistent

with our data. Similar arguments can be made against a role for prefrontal tDCS in speeding visual recognition, motor execution, or arousal.

## Conclusions

There has been some recent controversy over the efficacy of tDCS, as human behavioral findings have been questioned on methodological and statistical grounds [3, 6–8]. Our data, collected using the best available animal model of the human brain, show that tDCS affects brain connectivity. To the extent that tDCS increases “neural excitability,” it does so by modulating the timing of ongoing spiking activity instead of controlling the generation of action potentials. While this may preclude using tDCS at low current amplitudes to directly control individual neurons’ firing rates, it does suggest that tDCS may be a safe, low-cost, and effective therapy for disorders in which long-range neural communication is perturbed, as in schizophrenia [2], traumatic brain injury [54], and other diseases, or, using similar mechanisms to enhance cognitive performance in healthy individuals.

## STAR★METHODS

Detailed methods are provided in the online version of this paper and include the following:

- [KEY RESOURCES TABLE](#)
- [CONTACT FOR RESOURCE SHARING](#)
- [EXPERIMENTAL MODEL AND SUBJECT DETAILS](#)
- [METHOD DETAILS](#)
  - Animals and surgical preparation
  - Transcranial direct current stimulation
  - Behavioral task
- [QUANTIFICATION AND STATISTICAL ANALYSIS](#)
  - Analysis of behavioral data
  - Analysis of neural data

## SUPPLEMENTAL INFORMATION

Supplemental Information includes five figures and can be found with this article online at <https://doi.org/10.1016/j.cub.2017.09.020>.

## AUTHOR CONTRIBUTIONS

M.R.K., P.K.P., and C.C.P. designed the study. M.R.K. and T.P.Z. performed the experiments. M.R.K., T.P.Z., B.A.C., P.K.P., J.C., and M.E.P. analyzed the data. A.D. generated the stimulation montages. M.R.K. and C.C.P. wrote the paper.

## ACKNOWLEDGMENTS

This work was supported by the Defense Advanced Research Projects Agency (DARPA) via contract number N66001-14-C-4066 (transcranial Stimulation to Improve Memory: tSTIM) to P.K.P. and C.C.P. and a CIHR grant (MOP-115178) to C.C.P. We thank Drs. Barbara Jones and Adrien Peyrache for helpful discussions and Julie Coursol, Cathy Hunt, Michael D. Howard, and Dr. Fernando Chaurand for outstanding technical assistance. The views, opinions, and/or findings expressed are those of the authors and should not be interpreted as representing the official views or policies of the Department of Defense or the US Government. P.K.P., J.C., M.E.P., and A.D. have filed invention disclosures and have pending patent applications on various techniques and

applications of non-invasive stimulation. A.D. is employed by and owns equity in Soterix Medical, Inc., which aims to commercialize applications of HD-tDCS.

Received: March 19, 2017

Revised: July 19, 2017

Accepted: September 11, 2017

Published: October 12, 2017

## REFERENCES

1. Brunoni, A.R., Nitsche, M.A., Bolognini, N., Bikson, M., Wagner, T., Merabet, L., Edwards, D.J., Valero-Cabre, A., Rotenberg, A., Pascual-Leone, A., et al. (2012). Clinical research with transcranial direct current stimulation (tDCS): Challenges and future directions. *Brain Stimulat.* 5, 175–195.
2. Reinhart, R.M., Zhu, J., Park, S., and Woodman, G.F. (2015). Synchronizing theta oscillations with direct-current stimulation strengthens adaptive control in the human brain. *Proc. Natl. Acad. Sci. USA* 112, 9448–9453.
3. Mancuso, L.E., Ilieva, I.P., Hamilton, R.H., and Farah, M.J. (2016). Does transcranial direct current stimulation improve healthy working memory?: A meta-analytic review. *J. Cogn. Neurosci.* 28, 1063–1089.
4. Green, A.E., Spiegel, K.A., Giangrande, E.J., Weinberger, A.B., Gallagher, N.M., and Turkeltaub, P.E. (2017). Thinking cap plus thinking zap: tDCS of frontopolar cortex improves creative analogical reasoning and facilitates conscious augmentation of state creativity in verb generation. *Cereb. Cortex* 27, 2628–2639.
5. Kuo, M.F., Paulus, W., and Nitsche, M.A. (2014). Therapeutic effects of non-invasive brain stimulation with direct currents (tDCS) in neuropsychiatric diseases. *Neuroimage* 85, 948–960.
6. Hill, A.T., Fitzgerald, P.B., and Hoy, K.E. (2016). Effects of anodal transcranial direct current stimulation on working memory: A systematic review and meta-analysis of findings from healthy and neuropsychiatric populations. *Brain Stimulat.* 9, 197–208.
7. Horvath, J.C., Forte, J.D., and Carter, O. (2015). Quantitative review finds no evidence of cognitive effects in healthy populations from single-session transcranial direct current stimulation (tDCS). *Brain Stimulat.* 8, 535–550.
8. Horvath, J.C., Forte, J.D., and Carter, O. (2015). Evidence that transcranial direct current stimulation (tDCS) generates little-to-no reliable neurophysiologic effect beyond MEP amplitude modulation in healthy human subjects: A systematic review. *Neuropsychologia* 66, 213–236.
9. Antal, A., Keeser, D., Priori, A., Padberg, F., and Nitsche, M.A. (2015). Conceptual and procedural shortcomings of the systematic review “evidence that transcranial direct current stimulation (tDCS) generates little-to-no reliable neurophysiologic effect beyond mep amplitude modulation in healthy human subjects: A systematic review” by Horvath and Co-workers. *Brain Stimulat.* 8, 846–849.
10. Opitz, A., Falchier, A., Linn, G.S., Milham, M.P., and Schroeder, C.E. (2017). Limitations of ex vivo measurements for in vivo neuroscience. *Proc. Natl. Acad. Sci. USA* 114, 5243–5246.
11. Jackson, M.P., Rahman, A., Lafon, B., Kronberg, G., Ling, D., Parra, L.C., and Bikson, M. (2016). Animal models of transcranial direct current stimulation: Methods and mechanisms. *Clin. Neurophysiol.* 127, 3425–3454.
12. Radman, T., Su, Y., An, J.H., Parra, L.C., and Bikson, M. (2007). Spike timing amplifies the effect of electric fields on neurons: Implications for endogenous field effects. *J. Neurosci.* 27, 3030–3036.
13. Stagg, C.J., and Nitsche, M.A. (2011). Physiological basis of transcranial direct current stimulation. *Neuroscientist* 17, 37–53.
14. Zaehle, T., Sandmann, P., Thorne, J.D., Jäncke, L., and Herrmann, C.S. (2011). Transcranial direct current stimulation of the prefrontal cortex modulates working memory performance: Combined behavioural and electrophysiological evidence. *BMC Neurosci.* 12, 2.
15. Soekadar, S.R., Witkowski, M., Cossio, E.G., Birbaumer, N., Robinson, S.E., and Cohen, L.G. (2013). In vivo assessment of human brain

- oscillations during application of transcranial electric currents. *Nat. Commun.* **4**, 2032.
16. Keeser, D., Meindl, T., Bor, J., Palm, U., Pogarell, O., Mulert, C., Brunelin, J., Möller, H.J., Reiser, M., and Padberg, F. (2011). Prefrontal transcranial direct current stimulation changes connectivity of resting-state networks during fMRI. *J. Neurosci.* **31**, 15284–15293.
  17. Bindman, L.J., Lippold, O.C., and Redfearn, J.W. (1964). The action of brief polarizing currents on the cerebral cortex of the rat (1) during current flow and (2) in the production of long-lasting after-effects. *J. Physiol.* **172**, 369–382.
  18. Cosmo, C., Ferreira, C., Miranda, J.G., do Rosário, R.S., Baptista, A.F., Montoya, P., and de Sena, E.P. (2015). Spreading effect of tDCS in individuals with attention-deficit/hyperactivity disorder as shown by functional cortical networks: A randomized, double-blind, sham-controlled trial. *Front. Psychiatry* **6**, 111.
  19. Ozen, S., Sirota, A., Belluscio, M.A., Anastassiou, C.A., Stark, E., Koch, C., and Buzsáki, G. (2010). Transcranial electric stimulation entrains cortical neuronal populations in rats. *J. Neurosci.* **30**, 11476–11485.
  20. Márquez-Ruiz, J., Leal-Campanario, R., Sánchez-Campusano, R., Molaee-Ardekani, B., Wendling, F., Miranda, P.C., Ruffini, G., Gruart, A., and Delgado-García, J.M. (2012). Transcranial direct-current stimulation modulates synaptic mechanisms involved in associative learning in behaving rabbits. *Proc. Natl. Acad. Sci. USA* **109**, 6710–6715.
  21. Opitz, A., Paulus, W., Will, S., Antunes, A., and Thielscher, A. (2015). Determinants of the electric field during transcranial direct current stimulation. *Neuroimage* **109**, 140–150.
  22. Fries, P. (2015). Rhythms for cognition: Communication through coherence. *Neuron* **88**, 220–235.
  23. Datta, A., Krause, M.R., Pilly, P.K., Choe, J., Zanos, T.P., Thomas, C., and Pack, C.C. (2016). On comparing in vivo intracranial recordings in non-human primates to predictions of optimized transcranial electrical stimulation. *Conf. Proc. IEEE Eng. Med. Biol. Soc.* **2016**, 1774–1777.
  24. Kim, J.H., Kim, D.W., Chang, W.H., Kim, Y.H., Kim, K., and Im, C.H. (2014). Inconsistent outcomes of transcranial direct current stimulation may originate from anatomical differences among individuals: Electric field simulation using individual MRI data. *Neurosci. Lett.* **564**, 6–10.
  25. Petrides, M. (2005). Lateral prefrontal cortex: Architectonic and functional organization. *Philos. Trans. R. Soc. Lond. B Biol. Sci.* **360**, 781–795.
  26. Asaad, W.F., Rainer, G., and Miller, E.K. (1998). Neural activity in the primate prefrontal cortex during associative learning. *Neuron* **21**, 1399–1407.
  27. Datta, A., Bansal, V., Diaz, J., Patel, J., Reato, D., and Bikson, M. (2009). Gyri-precise head model of transcranial direct current stimulation: Improved spatial focality using a ring electrode versus conventional rectangular pad. *Brain Stimul.* **2**, 201–207.
  28. Huang, Y., Liu, A.A., Lafon, B., Friedman, D., Dayan, M., Wang, X., Bikson, M., Doyle, W.K., Devinsky, O., and Parra, L.C. (2017). Measurements and models of electric fields in the in vivo human brain during transcranial electric stimulation. *eLife*. Published online February 7, 2017. <https://doi.org/10.7554/eLife.18834>.
  29. Chukoskie, L., Snider, J., Mozer, M.C., Krauzlis, R.J., and Sejnowski, T.J. (2013). Learning where to look for a hidden target. *Proc. Natl. Acad. Sci. USA* **110** (Suppl 2), 10438–10445.
  30. Dalziel, C.F. (1954). The threshold of perception currents. *Electr. Eng.* **73**, 625–630.
  31. Bernstein, T. (1989). Investigation of alleged appliance electrocutions and fires caused by internally generated voltages. *IEEE Trans. Ind. Appl.* **25**, 664–668.
  32. Russo, R., Wallace, D., Fitzgerald, P.B., and Cooper, N.R. (2013). Perception of comfort during active and sham transcranial direct current stimulation: A double blind study. *Brain Stimulat.* **6**, 946–951.
  33. Gandiga, P.C., Hummel, F.C., and Cohen, L.G. (2006). Transcranial DC stimulation (tDCS): A tool for double-blind sham-controlled clinical studies in brain stimulation. *Clin. Neurophysiol.* **117**, 845–850.
  34. Okun, M., Naim, A., and Lampl, I. (2010). The subthreshold relation between cortical local field potential and neuronal firing unveiled by intracellular recordings in awake rats. *J. Neurosci.* **30**, 4440–4448.
  35. Hsu, T.Y., Juan, C.H., and Tseng, P. (2016). Individual differences and state-dependent responses in transcranial direct current stimulation. *Front. Hum. Neurosci.* **10**, 643.
  36. Nitsche, M.A., and Paulus, W. (2000). Excitability changes induced in the human motor cortex by weak transcranial direct current stimulation. *J. Physiol.* **527**, 633–639.
  37. Gamboa, O.L., Antal, A., Moliadze, V., and Paulus, W. (2010). Simply longer is not better: Reversal of theta burst after-effect with prolonged stimulation. *Exp. Brain Res.* **204**, 181–187.
  38. Fischer, B., and Boch, R. (1983). Saccadic eye movements after extremely short reaction times in the monkey. *Brain Res.* **260**, 21–26.
  39. Kobayashi, Y., Saito, Y., and Isa, T. (2001). Facilitation of saccade initiation by brainstem cholinergic system. *Brain Dev.* **23** (Suppl 1), S24–S27.
  40. Braun, D., and Breitmeyer, B.G. (1988). Relationship between directed visual attention and saccadic reaction times. *Exp. Brain Res.* **73**, 546–552.
  41. Fischer, B., and Breitmeyer, B. (1987). Mechanisms of visual attention revealed by saccadic eye movements. *Neuropsychologia* **25** (1A), 73–83.
  42. Beatty, J. (1982). Task-evoked pupillary responses, processing load, and the structure of processing resources. *Psychol. Bull.* **91**, 276–292.
  43. Bradley, M.M., Miccoli, L., Escrig, M.A., and Lang, P.J. (2008). The pupil as a measure of emotional arousal and autonomic activation. *Psychophysiology* **45**, 602–607.
  44. Zanos, T.P., Mineault, P.J., Nasiatou, K.T., Guitton, D., and Pack, C.C. (2015). A sensorimotor role for traveling waves in primate visual cortex. *Neuron* **85**, 615–627.
  45. Gregoriou, G.G., Gotts, S.J., Zhou, H., and Desimone, R. (2009). High-frequency, long-range coupling between prefrontal and visual cortex during attention. *Science* **324**, 1207–1210.
  46. Buschman, T.J., and Miller, E.K. (2007). Top-down versus bottom-up control of attention in the prefrontal and posterior parietal cortices. *Science* **315**, 1860–1862.
  47. Supèr, H., and Roelfsema, P.R. (2005). Chronic multiunit recordings in behaving animals: Advantages and limitations. *Prog. Brain Res.* **147**, 263–282.
  48. Ali, M.M., Sellers, K.K., and Fröhlich, F. (2013). Transcranial alternating current stimulation modulates large-scale cortical network activity by network resonance. *J. Neurosci.* **33**, 11262–11275.
  49. Creutzfeldt, O.D., Fromm, G.H., and Kapp, H. (1962). Influence of trans-cortical d-c currents on cortical neuronal activity. *Exp. Neurol.* **5**, 436–452.
  50. Cui, Y., Liu, L.D., McFarland, J.M., Pack, C.C., and Butts, D.A. (2016). Inferring cortical variability from local field potentials. *J. Neurosci.* **36**, 4121–4135.
  51. Reato, D., Rahman, A., Bikson, M., and Parra, L.C. (2010). Low-intensity electrical stimulation affects network dynamics by modulating population rate and spike timing. *J. Neurosci.* **30**, 15067–15079.
  52. Fellin, T., Pascual, O., Gobbo, S., Pozzan, T., Haydon, P.G., and Carmignoto, G. (2004). Neuronal synchrony mediated by astrocytic glutamate through activation of extrasynaptic NMDA receptors. *Neuron* **43**, 729–743.
  53. Monai, H., Ohkura, M., Tanaka, M., Oe, Y., Konno, A., Hirai, H., Mikoshiba, K., Itoharu, S., Nakai, J., Iwai, Y., and Hirase, H. (2016). Calcium imaging reveals glial involvement in transcranial direct current stimulation-induced plasticity in mouse brain. *Nat. Commun.* **7**, 11100.
  54. Sharp, D.J., Scott, G., and Leech, R. (2014). Network dysfunction after traumatic brain injury. *Nat. Rev. Neurol.* **10**, 156–166.
  55. Mitra, P., and Bokil, H. (2008). *Observed Brain Dynamics* (Oxford University Press).

56. Quiroga, R.Q., Nadasdy, Z., and Ben-Shaul, Y. (2004). Unsupervised spike detection and sorting with wavelets and superparamagnetic clustering. *Neural Comput.* *16*, 1661–1687.
57. Passingham, R.E., Toni, I., and Rushworth, M.F. (2000). Specialisation within the prefrontal cortex: The ventral prefrontal cortex and associative learning. *Exp. Brain Res.* *133*, 103–113.
58. Kobatake, E., and Tanaka, K. (1994). Neuronal selectivities to complex object features in the ventral visual pathway of the macaque cerebral cortex. *J. Neurophysiol.* *71*, 856–867.
59. Daw, N., and Courville, A.C. (2007). The pigeon as particle filter. *Adv. Neural Inf. Process Syst.* *20*, 369–376.
60. Gallistel, C.R., Fairhurst, S., and Balsam, P. (2004). The learning curve: Implications of a quantitative analysis. *Proc. Natl. Acad. Sci. USA* *101*, 13124–13131.
61. Zanos, T.P., Mineault, P.J., and Pack, C.C. (2011). Removal of spurious correlations between spikes and local field potentials. *J. Neurophysiol.* *105*, 474–486.

## STAR★METHODS

### KEY RESOURCES TABLE

REAGENT or RESOURCE	SOURCE	IDENTIFIER
Experimental Models: Organisms/Strains		
Rhesus macaque, <i>Macaca mulatta</i> (males, 4 and 10 years)	McGill University	N/A
Software and Algorithms		
MATLAB	The MathWorks, Natick, MA (USA)	v2016B
Chronux	<a href="http://chronux.org">http://chronux.org</a> , [55]	v2.10–2.12
WaveClust	[56]	N/A
Other		
Utah multielectrode arrays	Blackrock Microsystems, Utah (USA)	IrOx
PiSTIM tDCS electrodes	Neuroelectronics, Spain	N/A
Kwik-sil	World Precision Instruments	N/A
SignaGel Conductive Gel	Parker Laboratories	N/A

### CONTACT FOR RESOURCE SHARING

Further information and requests for resources should be directed to and will be fulfilled by the Lead Contact, Praveen Pilly ([pkpilly@hrl.com](mailto:pkpilly@hrl.com)).

### EXPERIMENTAL MODEL AND SUBJECT DETAILS

We obtained behavioral and neurophysiological data from two adult male rhesus macaque monkeys (*macaca mulatta*, 4 and 10 years old). All procedures were approved by the Animal Care Committee of the Montreal Neurological Institute and performed in accordance with guidelines established by the Canadian Council on Animal Care. Animals were housed under standard conditions with ad libitum food and a controlled light-dark cycle. Veterinary staff monitored the animals' health throughout the experiment.

All experiments described in this paper use a within-subject design, described below, so animals were not assigned to a specific experimental group.

### METHOD DETAILS

#### Animals and surgical preparation

We first acquired high-resolution (0.6–0.8 mm<sup>3</sup> voxels) T1 and T2-weighted anatomical MRIs for each animal. The T1 images were acquired using an MP RAGE pulse sequence (TR = 2300 ms, TE = 3.59 ms), while T2 images used a TR of 2800 ms and TE of 489 ms. We acquired 7–10 volumes per scan, which were denoised, aligned, and averaged offline using FSL and AFNI. These MRIs were used for surgical planning and to optimize tDCS electrode placement, as described below.

Using standard sterile surgical techniques, animals were then implanted with a customized titanium head post (Hybex Innovations, Montreal Canada). After an eight-week recovery period, they were familiarized with the laboratory environment, head fixation, and the behavioral task.

We attached MRI-opaque fiducial markers to the head post and acquired a second set of T1-weighted MRIs (as above). A second surgery was then performed to implant multi-electrode arrays (Blackrock Microsystems, USA) into the PFC and ITC. We targeted the ventrolateral PFC (areas 9/46v), based on its role in associative learning in humans [57] and monkeys [26]. Within ITC, we targeted area TEO, based on its role in representing complex visual stimuli [58].

The PFC and ITC were identified based on the MRI scans and a neuronavigation system (Brainsight Vet; Rogue Research Montreal Canada) that provided intraoperative positioning information, ensuring that arrays were accurately placed in each area. For each area, the skin and muscle overlying each target were retracted and a 15–20 mm bone flap was removed. Arrays were inserted with a pneumatic device and the bone flap was replaced and secured with titanium straps. The array connector was attached elsewhere on the skull, following the manufacturer's directions. The neuronavigation system was used to record the 3D positions of the arrays and other implanted objects (e.g., straps, bone screws, headpost). At the end of the implantation surgery, the skin was approximated to its original position and sutured.

### Transcranial direct current stimulation

The T1 and T2-weighted scans were annotated with the implants' positions and segmented into five tissue types (namely, gray matter, white matter, CSF, bone, skin). These data were used to generate a detailed finite element model of each monkey's head including all the intracranial and transcranial implants, which was then solved for electrode positions that maximize the tDCS-induced electric field strength in PFC while minimizing off-target stimulation and shunting through the implants [23]. When mapped back to a 10-20 human EEG layout, the montage for one monkey corresponds to Fp2 = +2 mA, O2 = -2 mA, and F4 = +2 mA, P7 = -2 mA for the other. These generated peak field strengths within PFC of 0.68 V/m and 0.42 V/m, respectively. Details of the modeling procedure and the montages for these monkeys have been published previously [23].

Transcranial direct current stimulation (tDCS) was performed using a commercially available system and a standard stimulation protocol [16], both of which are frequently used with human subjects (StarStim; Neuroelectronics). The 1 cm (radius) Ag/AgCl electrodes (PISTIM; Neuroelectronics) were coated with a conductive gel and attached to the scalp using a silicon elastomer (Kwik-Sil, World Precision Instruments). Electrode impedance was always below 10 k $\Omega$  and typically less than 2 k $\Omega$ .

During the passive fixation task, tDCS and sham stimulation were applied in 5 min blocks. The blocks were randomly ordered and separated by 5 to 10 min intervals. We collected at least ten blocks each day. For the foraging task, we pre-applied stimulation (tDCS or sham) for 5 min before the task began, then continued it until each image was presented 75 (monkey F) or 100 (monkey M) times. Because the task is self-paced, block lengths varied. The median stimulation time was 35 min (30 min for task execution, plus 5 min prestimulation), and stimulation was never applied for more than 1 hr. These blocks were separated by a 10-15 min interval and the tDCS/sham conditions were counterbalanced within and across days. Animals typically completed 1-3 blocks per day.

Since tDCS onset can produce somatosensory sensations, we used sham stimulation, rather than no stimulation, as a control. As in the active stimulation condition, the current was initially ramped up to 2000  $\mu$ A over three seconds. The stimulus was applied for 10 s, then ramped back down to 0 over three seconds; this process was repeated at the end of each block. This mimics the sensation of tDCS and ensures that any results are not due to changes in arousal or alertness from that sensation [33].

### Behavioral task

Animals were seated in front of a monitor that subtended 30  $\times$  60 degrees of visual angle at a viewing distance of 40 cm. Eye position and pupil area were monitored at 500 Hz with an infrared eye tracking system (SR Research; Ontario).

Our experimental paradigm was an adaptation of one previously shown to provide a useful probe of associative learning in humans [29]. Each trial began with the appearance of a black fixation spot on a gray screen. Animals were required to fixate within 2 deg. of the spot for 750-1000 ms, after which a full-screen image appeared. Images were chosen from a collection of Creative-Commons and public domain photographs of natural scenes and patterns ([flickr.com](http://flickr.com)). Different images were selected for every day of recording.

Within each image on each day, a small (2 $^\circ$  radius) patch at a random location was designated as the response zone (RZ). The RZ was initially not cued, and animals were allowed to freely view the image for 15 (Monkey F) or 20 s (Monkey M). If their gaze remained within the RZ for at least 100 ms, they received a large drop of juice and the trial ended. However, when subjects could not find the RZ within the allotted time, a high contrast cue appeared within it, and subjects received a much smaller reward for fixating the cue.

To increase the task difficulty, the RZ's position was jittered according to a bivariate normal distribution ( $\sigma = 1^\circ$  or  $4^\circ$ ). Each block contained 2-3 image/RZ pairs, presented 75-100 times each. The image order was randomized. We also interleaved control trials, in which the animal received a small reward for making a saccade to the same cue, presented against a neutral gray background. These trials ensured that the eye tracker remained calibrated and reduced carry-over effects between trials.

## QUANTIFICATION AND STATISTICAL ANALYSIS

Data processing and analysis were performed in MATLAB (The MathWorks, Natick, MA).

Except where specifically noted, statistical significance was assessed using randomization tests. Fisher-Pitman tests, which are analogous to t tests, were used to compare two sample data or matched pairs of data. When possible covariates were identified, a randomized F-test, akin to an ANOVA, was used instead. These tests make no assumptions about the distribution of the data, but require that data points be exchangeable under the null hypothesis. This requirement is easily met due to the design of our experiments. Results were identical when data were analyzed with classical t tests and ANOVAs instead. Where necessary, the p values reported here were adjusted for multiplicity using the Holm-Bonferroni method to maintain a familywise error rate of less than 5 percent."

### Analysis of behavioral data

We extracted the monkeys' RTs for all presentations of each image/RZ pair and smoothed them with a median filter (span = 3) to eliminate brief fluctuations in the monkeys' motivation and arousal. The data were well described by a sigmoidal function, so we fit the RT values to a model of the form:

$$RT(p) = -Gain \times \frac{1}{1 + e^{-slope \times (p - N_{50})}} + (Gain + MinRT)$$

where  $RT(p)$  is monkey's RT (in seconds) on the  $p$ -th presentation of an image/RZ pair. The models' parameters provide specific tests of several proposed tDCS effects. The  $MinRT$  parameter shifts the curve up and down. It corresponds to the subjects' asymptotic

performance: the total time needed to perform the task (i.e., to recognize the image, to retrieve the RZ location, and to execute an eye movement), once learning is complete. In contrast, the  $N_{50}$  parameter shifts the curve left and rightward, and represents the location on the abscissa where the animals' RT reaches half its asymptotic value. This therefore indicates the efficiency with which the animals learned. We disregard the *Gain* and *Slope* parameters. *Gain* is strongly influenced by the monkeys' luck on the first few trials. A detailed analysis of learning curves indicates that they often fail to reflect learning or memory acquisition, which often happens abruptly [59, 60]. Consistent with this, we found that a wide range of *Slope* values were consistent with qualitatively similar learning curves. Gallistel et al. [60] suggest ignoring the *Slope* parameter and instead focusing on time-to-criteria methods (like our  $N_{50}$  parameter), a recommendation we have followed in the rest of the paper.

We excluded sessions in which the logistic fits were inconsistent with on-task behavior ( $Gain < 3$  s or  $MinRT > 3$  s) or were physically implausible (offset  $< 0.5$  or  $N_{50} < 0$ , and  $N_{50} > 100$ ). These exclusions left us with  $n = 75$  sessions (38 tDCS, 37 sham). The excluded sessions were not preferentially associated with active tDCS or sham stimulation ( $p > 0.2$ , Fisher's exact test).

### Analysis of neural data

We recorded wideband signals from both arrays simultaneously using a Neural Interface Processor (Ripple, Salt Lake City, Utah). The signal was sampled at 30,000 Hz and band-pass filtered between 0.3 and 7500 Hz during acquisition. The data were subsequently processed offline to extract single-unit spiking activity and the local field potentials (LFPs). All analyses were performed with custom software written in MATLAB (The MathWorks, Natick, USA).

Single and multiunit activity were extracted by high-pass filtering the wideband signal (3<sup>rd</sup> order Butterworth,  $F_c = 500$  Hz). The resulting signal was thresholded at  $-3$  standard deviations (robustly estimated as 4.2 median absolute deviations). Single units' action potentials were sorted from segments around the threshold crossings using a wavelet-based clustering approach [56] and then manually reviewed for quality. The unsorted threshold crossings were also treated as multiunit activity, after imposing a 2-ms refractory period between adjacent threshold crossings.

We estimated the LFPs by low-pass filtering and down-sampling the wideband signal to 500 Hz, after using a Bayesian method [61] to remove powerline artifacts and contamination from nearby spikes. tDCS consists solely of DC current, and is therefore removed by the acquisition system's bandpass filter. Manual inspection confirmed that no stimulation artifacts were present in our data; ramp up and ramp down epochs do generate brief transients, but happened outside the behavioral task.

We performed our analyses on the 400 ms period following the onset of the visual scene in each trial. This was chosen to avoid confounds related to the strong influence of eye movements on LFPs [44]. To ensure that our results were not specific to this choice of analysis epoch, we repeated our analyses with data from the 400 ms period following the last saccade in each trial; results (not shown) were nearly identical.

From the data recorded on each trial, we extracted single-neuron activity and MUAs, LFP power, LFP-LFP coherence, MUA-LFP coherence. LFP power in frequencies ranging from 2-100 Hz was first calculated for each trial epoch on every electrode in PFC and ITC, and then averaged across electrodes and trial epochs to compute session averages for each area-epoch combination. We calculated LFP-LFP and LFP-MUA coherence using multi-taper methods [55], using three or four tapers (chosen on the basis of a preliminary analysis). Coherence was computed between all 18,336 pairs of electrodes. The coherence spectra were computed as a trial-averaged, within session values, numerically integrated to find the average power within each frequency band, and then averaged across electrodes and sessions.

Since little is known about the stimulus features encoded by PFC and ITC neurons, we used a linear discriminant analysis (LDA) to assess changes in neuronal selectivity (Figure 5B). LDA classifiers were trained separately for each experimental session and brain area. Each classifier used the per-trial activity from well-isolated single units ( $n_{ITC} = 18.8 \pm 1$ ,  $n_{PFC} = 11.0 \pm 0.6$  per session) or MUA recorded on all electrodes within an area during the analysis windows as inputs, and attempted to predict the identity of the image shown during that trial. Individual classifiers' performance was evaluated by averaging the test set results from 500 repeats of 10-fold cross-validation. As a control, classifiers were also trained on data in which the scene labels were shuffled across observations; these runs produced the expected 50% classification rate.

Generalized linear models were used to determine whether LFP power and coherence were associated with changes in the animals' behavior. Predictor variables were centered and scaled on a per-animal basis before model fitting. The GLM used a normal (Gaussian) probability distribution, with a logarithmic link function, matching the strictly positive domain of the response variable ( $N_{50}$ ). A reanalysis of the data using an identity link and/or gamma distribution yielded very similar results and residuals (not shown).

To assess their predictive power, models were compared, via a F test, to a constant model containing only an intercept. We assessed the significance of variables in two ways. Confidence intervals around individual coefficients were tested to see if they included or excluded zero. This was verified using a model selection approach [50], where the Bayesian Information Criterion was calculated for the full model as well as a series of reduced models where each parameter was removed in turn. Predictors leading to large increases in BIC ( $>10$ ) are considered as providing important information about the response variable.

**Current Biology, Volume 27**

**Supplemental Information**

**Transcranial Direct Current Stimulation**

**Facilitates Associative Learning and Alters**

**Functional Connectivity in the Primate Brain**

**Matthew R. Krause, Theodoros P. Zanos, Bennett A. Csorba, Praveen K. Pilly, Jaehoon Choe, Matthew E. Phillips, Abhishek Datta, and Christopher C. Pack**

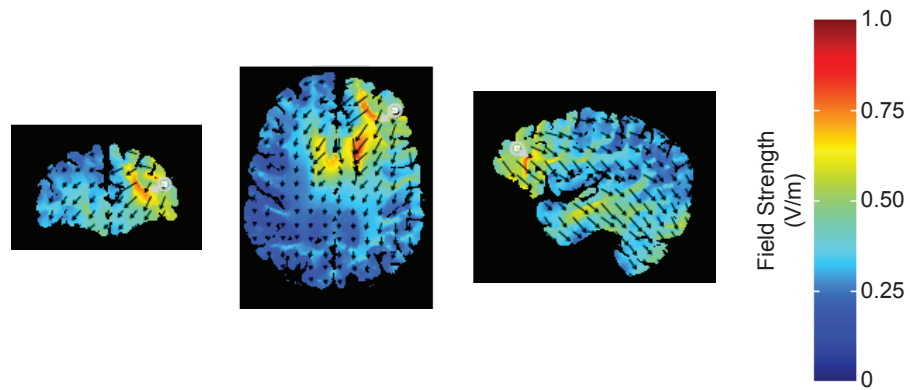


**Figure S1. Electric field maps.** A finite element model of each monkey's head was generated from structural MRIs and intraoperative records. It was then solved for electrode positions that maximize current flow through a specified brain area. In this example, we sought to maximize current flow through monkey M's PFC (grey square), for the experiment in Figure 1 and Figure 2A. Colors indicate the strength of the induced field, arrows indicate the current's direction. For additional details, see [S1], as well as the Results and Methods section.

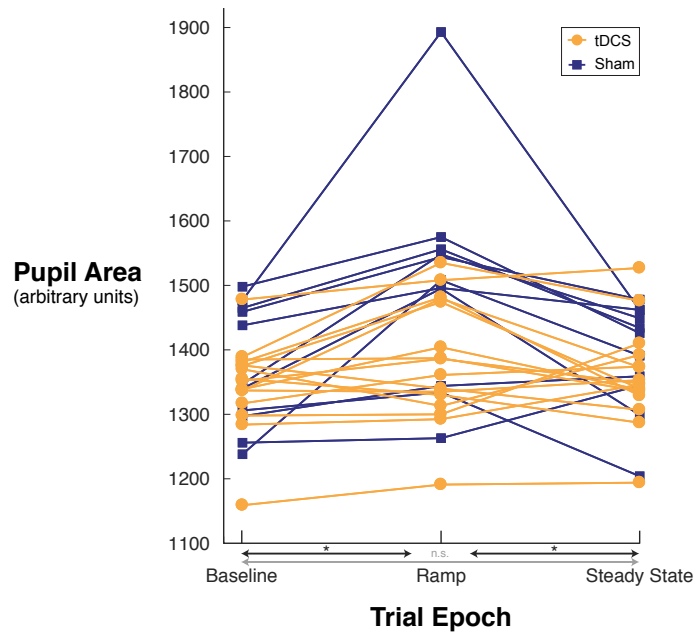


**Figure S2. Stimulation causes only transient changes in pupil area.** Pupil area trajectories are shown for epochs before the onset of stimulation (“baseline”), while stimulation current is ramped up (“ramp”) and once current reaches its steady state of 2 mA, in tDCS blocks, or 0 mA in sham blocks (“steady state”). Visual stimulation is held constant across all three epochs. Pupil area is significantly increased during the ramp phase, relative to the baseline, but returns to baseline once the current reaches steady state. Asterisks indicate  $p < 0.001$  (see main text for details and numbers). Color indicates stimulation/sham condition (no significant difference between baseline and steady state was observed). Error bars indicate the standard error of the grand mean.

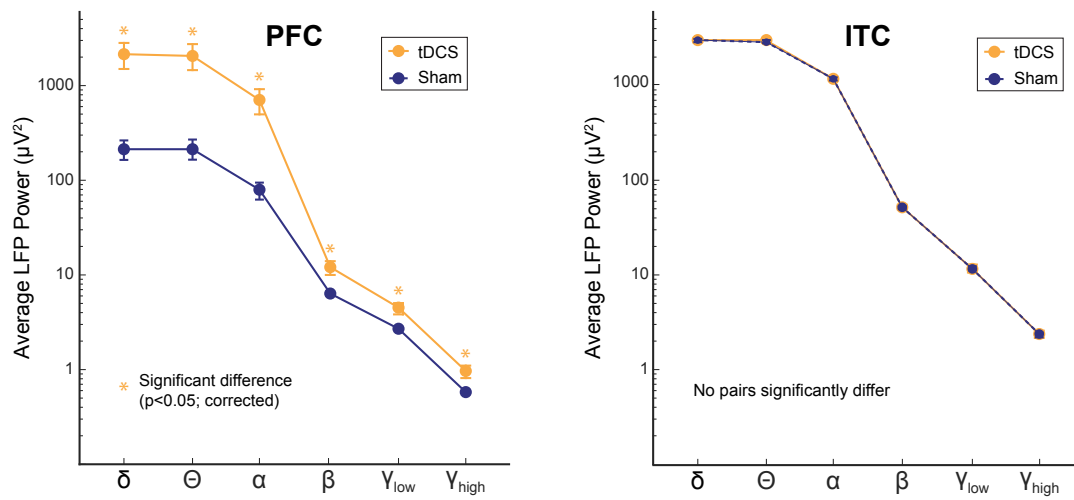


**Figure S3. tDCS increases LFP spectral power in PFC during behavior.** Main Figure 4 shows the *change* in LFP power with stimulation. Here, we plot the average values for both tDCS and sham conditions within one monkey. \* indicates pairwise differences that are significant at a corrected 0.05 level (via randomized F tests). See main text and Main Figure 4 for details; color indicates stimulation condition, while error bars indicate the standard error of the grand mean.

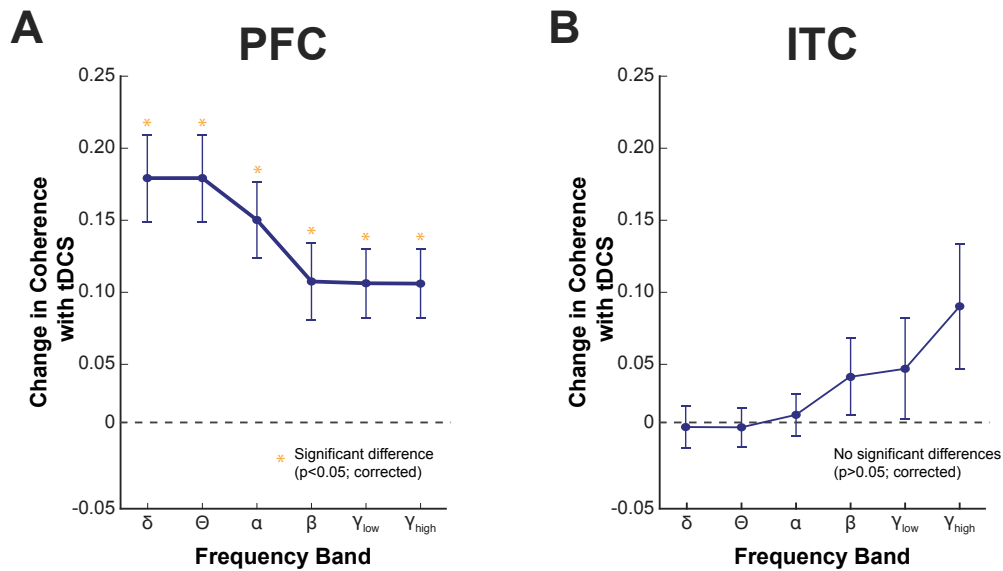


**Figure S4. tDCS alters functional connectivity within the stimulated areas.** The difference between LFP-LFP coherence for tDCS and sham conditions within each array (see also Main Figure 6, which compares data across areas). Positive values indicate greater coherence during tDCS; negative values indicate greater coherence during sham sessions, and error bars indicate the standard error of the *difference* of the grand means for each condition. When tDCS was applied, coherence significantly increased in all frequency bands in PFC (\* denotes  $p < 0.05$ , corrected). However, no significant changes were observed in ITC in any frequency bands. See Main Figure 6 for coherence between areas.

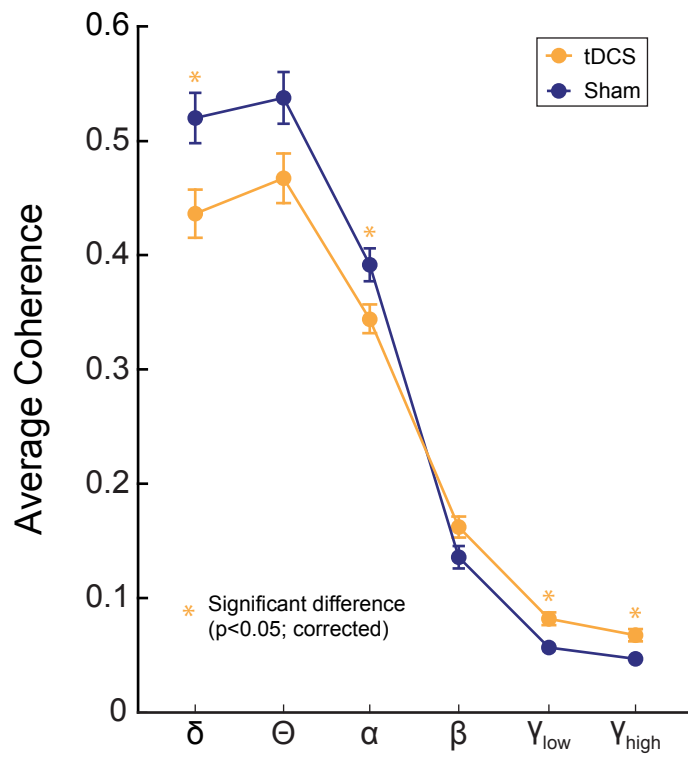


**Figure S5. tDCS alters functional connectivity between brain areas.** Main Figure 6 shows the *change* in LFP-LFP coherence between PFC and ITC with stimulation. Here we plot the average values for each condition.\* indicates pairwise differences that are significant at a corrected 0.05 level, while error bars denote the standard error of the grand mean. See main text and Figure 6 for details

## Supplemental Reference

[S1]. Datta, A., Krause, M.R., Pilly, P.K., Choe, J., Zanos, T.P., Thomas, C., and Pack, C.C. (2016). On comparing in vivo intracranial recordings in non-human primates to predictions of optimized transcranial electrical stimulation. *Proceedings of the 38th Annual International Conference of the IEEE Engineering in Medicine and Biology Society*.